

IET Renewable Power Generation

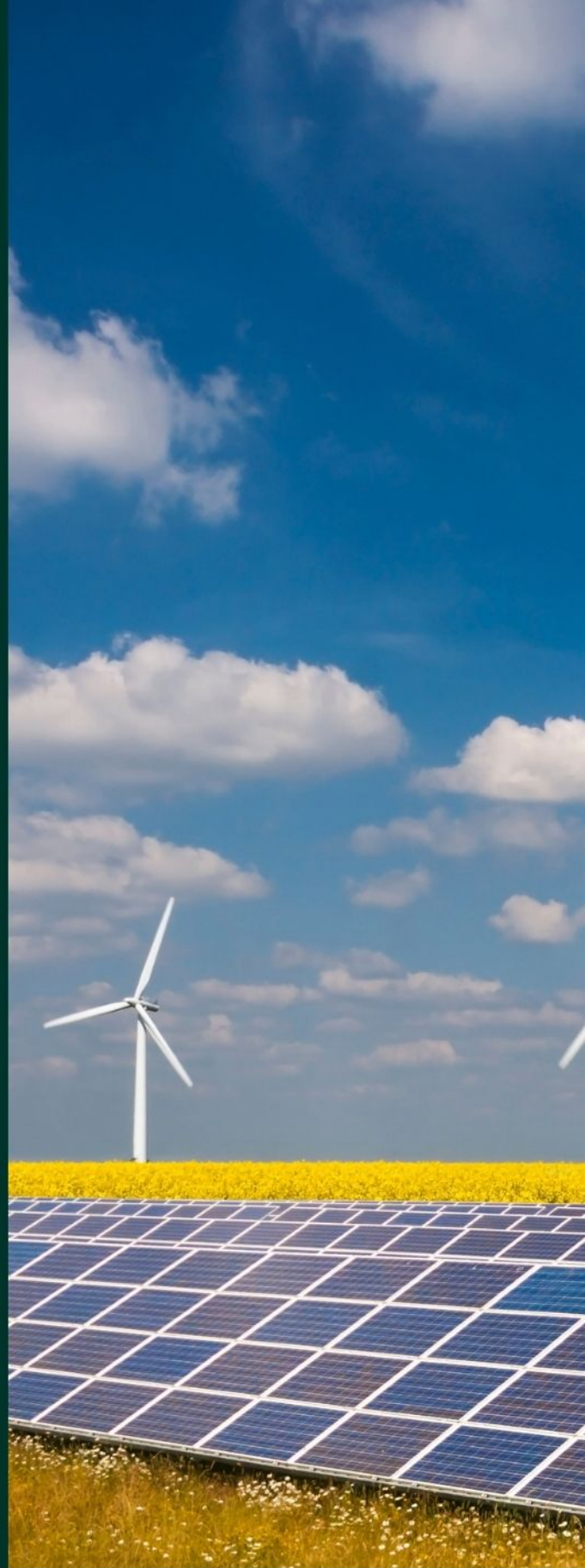
Special Issue Call for Papers

**Be Seen. Be Cited.
Submit your work to a new
IET special issue**

Connect with researchers and
experts in your field and
share knowledge.


Be part of the latest research
trends, faster.

[Read more](#)



The Institution of
Engineering and Technology

Experimental analyses of two-body wave energy converters with hydraulic power take-off damping in regular and irregular waves

Shuang Wu^{1,3}  | Yanjun Liu^{1,2,3} | Jian Qin^{1,3}

¹ Institute of Marine Science and Technology, Shandong University, Qingdao, Shandong 266237, China

² School of Mechanical Engineering, Shandong University, Jinan, Shandong 250100, China

³ Key Laboratory of High Efficiency and Clean Mechanical Manufacture of Ministry of Education, Shandong University, Jinan, Shandong 250100, China

Correspondence

Yanjun Liu, Institute of Marine Science and Technology, Shandong University, Qingdao 266237, Shandong, China.
Email: lyj111ky@163.com

Funding information

National Nature Science Foundation of China, Grant/Award Number: U1706230; National Key R&D Program of China, Grant/Award Number: 2016YFE0205700

Abstract

A flume experimental study of a two-body wave energy converter (WEC) with a hydraulic power take-off (PTO) was conducted under the conditions of both regular and irregular waves. The experimental results were analysed using the control variable method, and the effects of the wave elements and external load on the relative heave motion response and capture width ratio of the device are discussed. For the regular waves, three modes were found when analysing the variation of the relative heave motion response with the incident wave height, and the initial moving line of the WEC model was obtained. For the irregular waves, the experiment displayed two motion states. One was a following motion with a similar value to the incident wave period, and the other was a delayed motion with a larger value than the wave period. Based on the calculation of the capture width ratio of the system both under the regular and irregular wave conditions, the maximum value occurred at a frequency ratio of $\omega/\omega_n = 0.59$ and a hydraulic load of $p = 0.20$. The capture width ratio in the irregular waves was approximately 10%–40% higher than that of the regular waves for the same wave parameters.

1 | INTRODUCTION

The huge energy potential carried by ocean waves has deeply attracted the attention of researchers [1–3]. The utilization of wave energy can be traced back to more than 200 years ago, and after the rapid development in recent decades, hundreds of wave energy converters (WECs) have been developed so far [4]. There are three main types according to the capture mode: oscillating types, oscillating water column, and the overtopping device. Many literatures have introduced in detail [5–11]. Among them, the oscillating types of WECs, which account for the largest proportion, are characterized by the relative movement between a single floating body and the seabed or between two or more floating bodies. Compared with the single-body devices, the two-body WEC is easier to moor in deep water, allowing the device to go to the deep sea and be installed in a position with better wave conditions. Moreover, the synergistic effect between the two-body device is considered to have better energy capture characteristics than a single-body device [12]. There are also many types of PTO systems for WECs,

such as air turbines, water turbines, hydraulic systems, and linear motors. The hydraulic type PTO is the most commonly used, as they are well adapted to waves with large forces and slow speeds [13–15].

The theoretical study of the two-body WEC is typically simplified to two cylindrical floats, both of which experience heave motions under the excitation of regular waves. Based on the linear potential flow theory, the Eigen function expansion method and the separate variable method have been used to study the diffraction and radiation effects, without the consideration of the external load [16–18]. The dynamic response and capture width ratio were analysed using the frequency domain and time domain equations, and the external load was considered. Weinstein et al. analysed the operation characteristics of two floats with the same diameter under linear load damping, and the results showed that wave frequency was the primary factor that affected the capture width ratio of such a type of converter [19–21]. Candido (2011b) also based his study on a similar model to investigate the optimal values of linear external loads at different wave frequencies and the influence on the capture

This is an open access article under the terms of the [Creative Commons Attribution](https://creativecommons.org/licenses/by/4.0/) License, which permits use, distribution and reproduction in any medium, provided the original work is properly cited.

© 2021 The Authors. *IET Renewable Power Generation* published by John Wiley & Sons Ltd on behalf of The Institution of Engineering and Technology

width ratio [22]. Wu Bijun et al. [23] and Lin Liqun et al. [24] established the heave motion equation of a double cylindrical model with different diameters, analysed its capture width ratio characteristics under the action of linear loads, and studied the influence of vertical spacing between two bodies. Wachter et al. [25] and Ruehl [26] established the time-domain equation of heave motion of two floats with the same diameter, and they analysed the influence of nonlinear external load damping force and energy storage regulator on the operation characteristics of the WEC model. Chau, F. P. solved the radiation problem of a WEC with two concentric vertical cylinders using analytical solutions with the PTO system simplified as an equivalent linear damping proportional to the relative heave velocities [27]. I.H. Cho extends it to include diffraction problems [28]. Zheng et al. evaluated the maximum power absorption of two interconnected floaters using a mathematical model based on the 3D wave radiation-diffraction theory [29]. More recently, Zheng et al. presented a WEC consisting of a floating hollow cylinder capped by a roof with a variable aperture and a linear generator power take-off. They investigated the hydrodynamic characteristics of this WEC using an analytical model based on the potential flow theory [30]. Liang and Zuo [12] studied the dynamics of a two-body system and considered both the linear viscous damping and the hydrodynamic damping adopting a linearized model in the frequency domain. They found closed-form solutions for both an optimal and suboptimal PTO. On the basis, Peng Jin et al. [31] further considered the coupling effect of the hydrodynamic coefficients. The above theoretical research results are helpful to better understand the performance of a two-body WEC. However, further by experimental studies are still required.

Initially experimental studies of oscillating types WEC have predominantly focus on single-body structures, and few studies involving two-body WECs have been performed [32–36]. In most cases, large-amplitude relative motions will result in significant nonlinearity, which enhances the difficulty of understanding and analysing a system. The primary limitation is the inability to consider water loss due to real (viscous) fluid effects (large eddy turbulence), and the inability to accurately simulate large amplitude water oscillations (non-linear waves) [37]. Therefore, it is necessary to conduct some small-scale tests under laboratory conditions by isolating some dynamic effects. Yang [38] conducted a flume experiment study on the motion of two cylindrical buoys connected by a piston cylinder, and they preliminarily discussed and analysed the influence of the wave elements, the external load, the buoy arrangement, and the anchorage

with a feedback controlled linear actuator under the conditions of both regular and irregular waves, and they explored the influence of the different types of floating bodies on the power and capture width characteristics of the system. Sung-Jae Kim et al. [41] measured various viscous damping and energy losses from a WEC system and the hydraulic cylinder pressure of a PTO system. The experimental model was a buoy WEC system that was connected directly to a fixed platform. Son et al. [42] and Jin et al. [43] both experimental studied a dual coaxial-cylinder WEC with a direct-drive linear generator under various wave conditions, and the optimum parameters of the generator were determined using this systematic experimental research.

The published experimental studies have primarily focused on a WEC model with a direct-drive generator load, and test studies of a two-body WEC with hydraulic loads are rare. However, there are few studies that have investigated the effect of hydraulic PTO damping on the behaviour and power performance of a two-body WEC. In some experiments, servo valves were typically used to control the reciprocating movement of the hydraulic cylinder to simulate the wave input, which cannot truly reflect the operating state of a WEC in the wave [44]. Furthermore, there have been a few efforts to investigate two-body WEC tests in irregular waves (closer to a real marine environment), and the quantitative analysis of irregular waves by comparing with the results of regular waves is also worth studying.

In this study, a series of flume experiments are conducted on a typical two-body WEC. The WEC geometry used was inspired by the Ocean Power Technologies PowerBuoy [45] (Figure 1). The two bodies were connected by a hydraulic cylinder to realize the conversion of kinetic energy to hydraulic energy, and the hydraulic load was variable. A data acquisition system was designed to record the key parameters, such as displacement, pressure, and flow rate, during the operation of the test model, so as to explore and compare the dynamic characteristics of the device under regular and irregular waves.

2 | EXPERIMENTAL METHODOLOGY

2.1 | Basic model and parameter calculation

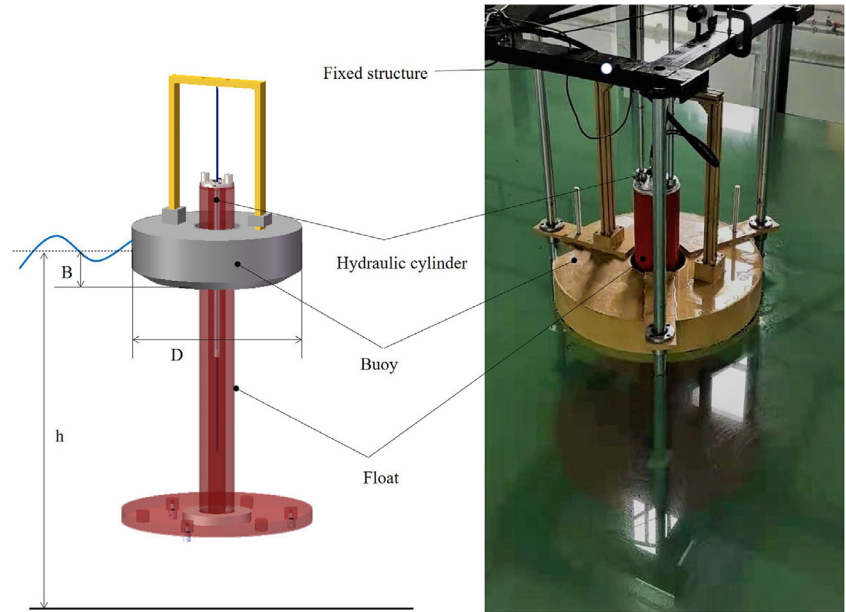
As the absorption of wave energy primarily depends on the relative heave motion between the buoy and float, only the heave motion is considered in this study. Using the linear potential theory and Newton's second law, the motion functions of the two are as follows [46]:

$$\begin{cases} (M_1 + M_{11}) \ddot{x}_1 + C_{11} \dot{x}_1 + K_1 x_1 + M_{12} \ddot{x}_2 + C_{12} \dot{x}_2 + C |\dot{x}_1 - \dot{x}_2| + \frac{F_d}{2} \left(1 + \frac{\dot{x}_1 - \dot{x}_2}{|\dot{x}_1 - \dot{x}_2|} \right) = F_1 \\ (M_2 + M_{22}) \ddot{x}_2 + C_{22} \dot{x}_2 + K_2 x_2 + M_{21} \ddot{x}_1 + C_{21} \dot{x}_1 + C |\dot{x}_1 - \dot{x}_2| + \frac{F_d}{2} \left(1 + \frac{\dot{x}_1 - \dot{x}_2}{|\dot{x}_1 - \dot{x}_2|} \right) + F_m = F_2 \end{cases} \quad (1)$$

mode on the operational characteristics. The test was conducted under a regular wave condition only. Beatty et al. [39, 40] conducted experiments using two variations of a two-body WEC

where M_1 , M_{11} , C_{11} and K_1 are the mass, added mass, added damping coefficient, and hydrostatic restoring stiffness caused

FIGURE 1 Schematic diagram of the two-body WEC



by the buoy's heave motion, respectively. The same meaning applies to the float. M_{12} and C_{12} are the heave added mass and radiation damping of the floating body acting on the buoy by relative motion, respectively; M_{21} and C_{21} are the heave added mass and radiation damping of the buoy acting on the float by relative motion, respectively; C is the damping coefficient of the inner wall of the piston cylinder; \dot{x}_i , \dot{x}_i and \ddot{x}_i ($i = 1, 2$) are the displacement, velocity, and acceleration of the heave motion of the buoy and float, respectively; F_1 and F_2 are the wave excitation force acting on the buoy and the float body respectively; F_a is the load exerted on the WEC by the hydraulic energy system, Falcao [47] simplified the force like the coulomb damping force. The mathematical expression is: $F_a = -\text{sign}(\dot{x}_1 - \dot{x}_2)P_s$, Where s_c is the sectional area of a hydraulic cylinder, P is load pressure. F_a is in the opposite direction of the relative velocity. In this flume test, P can be loaded by the designed hydraulic circuit, and the variable range of P value is 0–10 MPa. The WEC test model outputs hydraulic energy only when the interaction between the two bodies can overcome the applied load within the unit wave period. F_m represents the vertical motion constraint on the float.

The wave energy absorption rate is typically quantified in terms of the capture width ratio. It can be calculated using the following equation:

$$\eta = E_b/E_0 \times 100\% \quad (2)$$

where E_0 is the energy provided by the incident wave in a unit wave period and can be obtained using the equation found in Falnes [48]; and E_b is the hydraulic energy converted by the wave energy converter during a unit wave period.

$$E_0 = \frac{1}{8}\rho g H^2 \lambda D \cdot \frac{1}{2} \left(1 + \frac{2kH_w}{\sinh(2kH_w)} \right) \quad (3)$$

$$E_b = PQT \quad (4)$$

where k and H_w represent the wave number and water depth, respectively; and T is the incident wave period and pressure P . The flowmeter, Q , can be obtained directly by the experimental observations.

The relative motion displacement, Z , of the floating body and the capture width ratio of the system are the primary parameters used to describe the dynamic performance of the two-body system, which are affected by several factors. It mainly includes the incident wave height, H , the incident wave period, T , the model diameter, D , the system damping, c , and the external load, P . In order to characterize the universality of the experimental results, based on the theory of dimensional homogeneity, the following dimensionless parameters were used to describe the experimental results:

$$Z/H = f_1'(H/B, \omega/\omega_n, p \dots) \quad (5)$$

$$\alpha/2\pi = f_2'(H/B, \omega/\omega_n, p \dots) \quad (6)$$

$$\eta = f_3'(H/B, \omega/\omega_n, p \dots) \quad (7)$$

where α is the phase difference between the relative displacement and the wave elevation. The $p = P/P_{\max}$ and P_{\max} is the maximum external load that can be applied by the experimental system. In this study, it is 10 MPa; B is the draft depth of the buoy; ω is the wave frequency which can be calculated from wave period $\omega = 2\pi/T$; ω_n is the natural frequency of the model, which can be obtained from the hydrostatic decay test. In the flume experiments, the water depth was maintained at a constant, and the effects of H/B , ω/ω_n , and p on Z/H and η are quantitatively analysed.

2.2 | Experimental setup and conditions

The experimental study was conducted in the underwater equipment laboratory of the Qingdao Haijian Group. Details of the

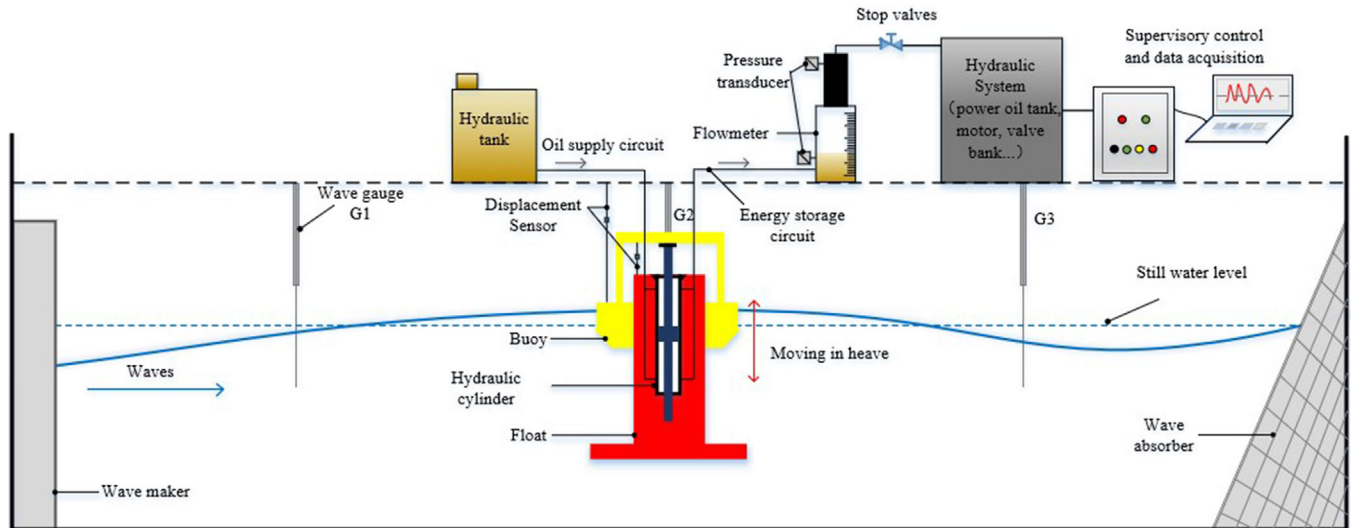


FIGURE 2 Sketch of the experimental setup in the wave flume

TABLE 1 Tank specifications

Parameter	Value	Units
Length	30.00	m
Width	4.00	M
Height	3.50	m
Maximum water depth	2.00	m
Wave height range	0.02–1.00	m
Wave period range	1.00–3.00	s

flume are listed in Table 1. The tank operated a piston-type wave maker composed of ten independent panels, and it is able generate incident waves up to 1.0 m in wave height with a range of wave periods from 1.0–3.0 s. The wave absorber was a slope built by the wave suppression network that was used to prevent reflected waves. When the maximum diameter of the model was no greater than 1/5 of the tank width, the hydrodynamic influence of the tank wall could be ignored [49, 50]. The model was installed in the centre of the pool, and the experimental water depth h was 2 m and remained constant. The buoy was a conical table with an outer diameter of $D = 0.8$ m, a total height of 0.25 m, and a draft depth of $B = 0.12$ m in still water. The float body had a diameter of 0.17 m, a height of 1.3 m and was connected to a damping disc with a diameter of 0.8 m and a thickness of 0.1 m. The mass of the buoy and float was 28.57 and 51.79 kg, respectively. The device was connected with a guide bracket fixed at the bottom of the flume that restricted the model moving during heaves only.

To measure the incident wave height, three wave gauges were installed seven meters in front of the model, seven meters behind the model, and parallel to the model to record the wave parameters in real time during the experiment. Displacement sensors were installed between the two bodies and above the centre of the buoy to record the relative motion displacement and the buoy motion displacement.

The double-acting hydraulic cylinder as the PTO component was installed inside the float, and its piston rod was connected to the portal frame of the buoy so as to realize the transfer of the relative motion energy. The inner diameter of the hydraulic cylinder was 0.02 m, the diameter of the piston rod was 0.01 m, and the effective stroke was 0.8 m. A total of four hydraulic oil channels are connected with the hydraulic cylinder. The oil supply circuit provides the hydraulic load and the energy storage circuit output hydraulic energy. The pressure acquisition system and the flow meter measured the pressure and flow in the PTO system. The developed test system synchronously recorded the acquisition parameters, and the sampling frequency was 30 Hz. The extracted wave energy was calculated from the hydraulic pressure and flow rate of the cylinder during the relative motions. Figures 2 and 3 show the overall schematic diagram and a test site picture of this experiment, respectively. A hydrostatic decay test was first performed in order to obtain the natural frequency of the model system. To perform the decay test, the two-body model was lifted with an initial displacement of $H_{in} = 0.2$ m in still water without a hydraulic load, by recording the displacement, H_{decay} , for several oscillation periods (Figure 4), and the natural decay period was found to be around 1.3 s (frequency = 4.833 rad/s).

3 | TEST RESULTS AND DISCUSSIONS

3.1 | Regular waves

3.1.1 | The relative heave motion response

Figure 5(a–e) shows the time histories of the wave elevation, $a(t)$, the relative heave motion, $\zeta(t)$, and the instantaneous relative velocity, $u(t)$, during regular waves under different external hydraulic loads. The wave conditions were $H/B = 1.67$ and $\omega/\omega_n = 0.72$. The instantaneous velocity curve, $u(t)$, was



FIGURE 3 Device in the flume

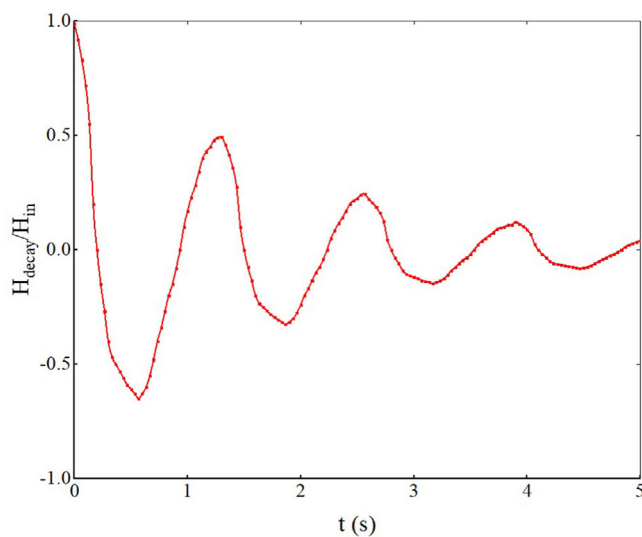


FIGURE 4 Heave decay from the experimental measurement

calculated from the derivative of the relative displacement with respect to time t . It can be seen from the curves that the period of the relative motion was basically the same as the incident wave period, and the maximum amplitude of the relative motion displacement and instantaneous velocity decreased with an increase in the hydraulic load. For the load pressure $p = 0, 0.06, 0.12$ (see Figure 5(a–c)), the relative motion amplitude was larger than the incident wave amplitude. This was because the buoy and float bodies could move in the opposite direction at the same frequency. The phase difference between the instantaneous velocity and the elevation of the incident wave was also affected by the value of the load. For the load $p = 0$ (see Figure 5(a)), the phase difference was approximately equal to $\pi/2$. With an increase in the load, the phase difference was gradually reduced, that is, to the direction of resonance.

The maximum heave displacement of the relative motion is an important parameter to characterize the motion response of a two-body WEC. In most of the published papers, the PTO model has typically been simplified. Figure 6(a) compares the

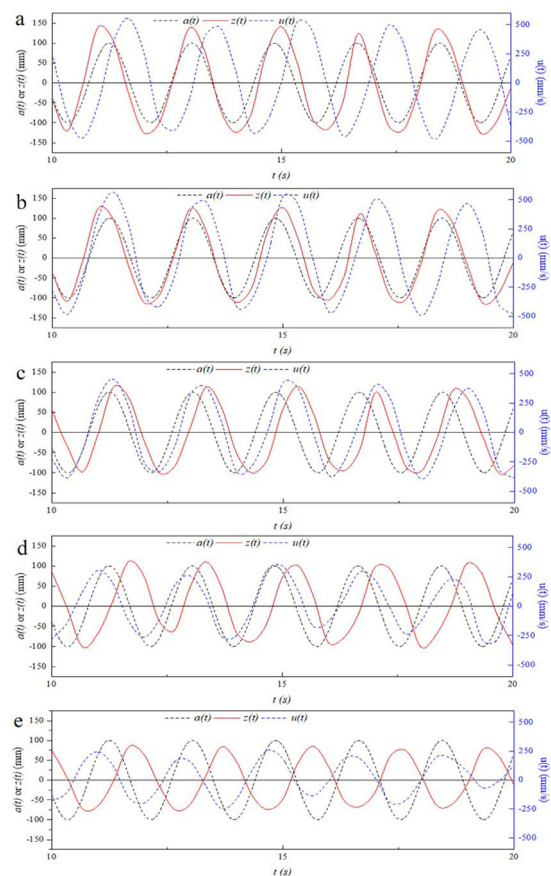


FIGURE 5 Time histories of the wave elevation $a(t)$, relative heave motion $z(t)$ and relative velocity $u(t)$ in regular waves, $H/B = 1.67$, $\omega/\omega_n = 0.72$, hydraulic load: (a) $p = 0$, (b) $p = 0.06$, (c) $p = 0.12$, (d) $p = 0.30$, (e) $p = 0.60$

maximum relative heave displacement varying with the incident wave frequency under three hydraulic PTO load values ($p = 0, 0.12$, and 0.30) obtained from experimental tests. The wave heights are $H/B = 1.67, 2.08$ and 2.50 . The test results show that, within the range of the parameters selected in the figure, the wave height had no significant effect on the maximum relative heave displacement. It can be seen that with an

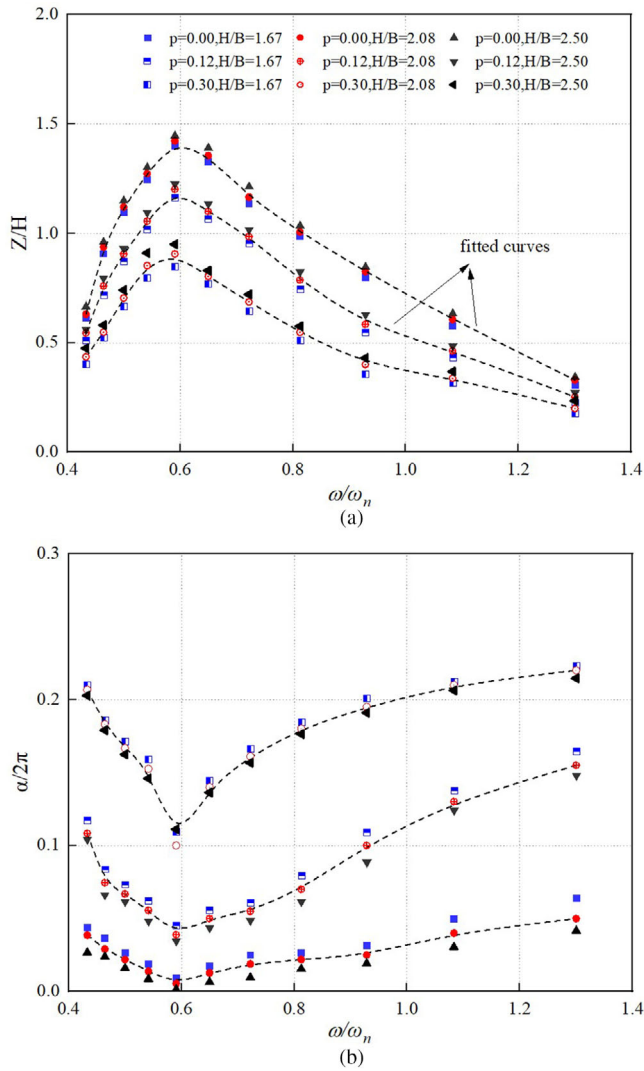


FIGURE 6 Variations of (a) maximum relative heave displacement Z/H and (b) phase difference $\alpha/2\pi$, with ω/ω_n in regular waves. The dashed lines are fitted curves of the measured data points

increase in the H/B , the value of Z/H increased slightly under the same wave frequency. However, the effect of the wave frequency was more considerable. Under all of the load conditions, Z/H increased first and then decreased with frequency during a single peak curve. For $\omega/\omega_n = 0.59$, the Z/H reached the maximum, and with an increase in the load, the maximum heave displacement amplitude decreased. Figure 6(b) shows the variation of $\alpha/2\pi$ with ω/ω_n for three values of p and incident wave heights. $\alpha/2\pi$ has the opposite trend with the increase of ω/ω_n as Z/H shown in Figure 6(a). In the range of test parameters, the phase difference between the relative displacement and the wave elevation is the smallest when the amplitude of the relative displacement reaches the maximum. The minimum value is close to zero. Under the same wave conditions, the higher the hydraulic load value, the smaller the phase difference.

Based on Figure 6, Figure 7 further expands the parameter range of the wave height, the variation in relative motion

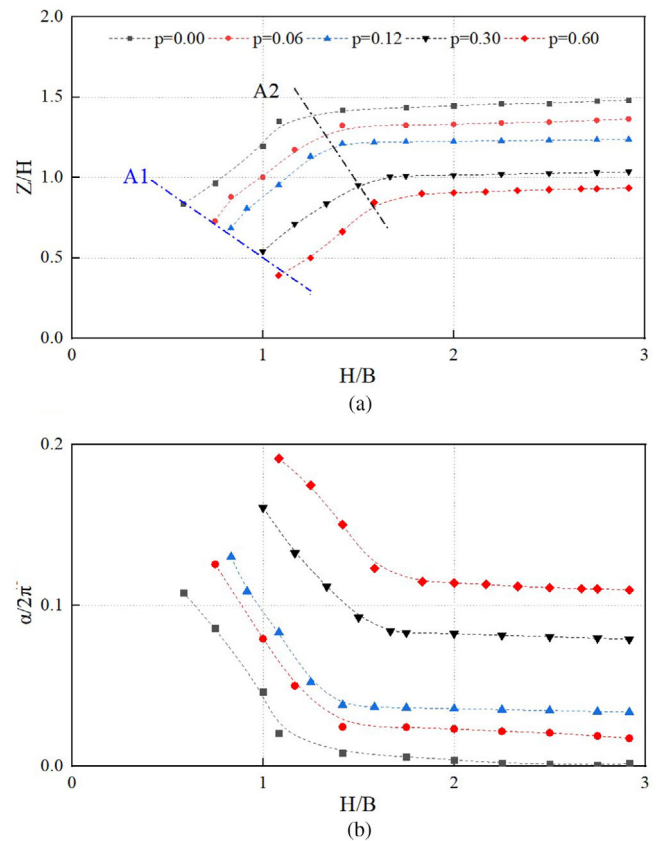


FIGURE 7 Variations of (a) maximum relative heave displacement Z/H and (b) phase difference $\alpha/2\pi$, with H/B in regular waves at $\omega/\omega_n = 0.59$

response with the wave height under different PTO loads was analysed. The frequency of the incident wave was maintained at $\omega/\omega_n = 0.59$. Two guides, A1 and A2, were added to divide the graph into three regions, as shown in Figure 7(a). First, in the region to the left of the line A1, the relative motion did not occur, that is, $Z/H = 0$. Therefore, it can be concluded that the auxiliary line, A1, was the initial moving line of the two-body WEC, and the starting wave height value increased with an increase in the external load. In the region between the two auxiliary lines, A1 and A2, the value of Z/H changed non-linearly with H/B . To be precise, within this range, the wave height had a significant effect on the relative motion displacement, which further supplemented the results in Figure 6. In the third region, to the right of line A2, the Z/H line tended to be horizontal. That is to say, there is a critical value of H/B as shown by the auxiliary line A2, over which Z/H remains approximately constant, meaning that a linear relationship was established between the relative motion and the height of the incident wave. With an increase in the hydraulic load value, the linear motion appeared when the H/B value was larger. For example, for $p = 0$, the Z/H remained constant when the H/B is larger than 1.26; while for $p = 0.60$, the Z/H remained constant when the H/B is larger than 1.58. Figure 7(b) shows the corresponding values of $\alpha/2\pi$ varying with H/B for different damping ratios. For a given load value, there is no motion of the buoy at small values of H/B . With increasing H/B , the phase difference shows non-linearity

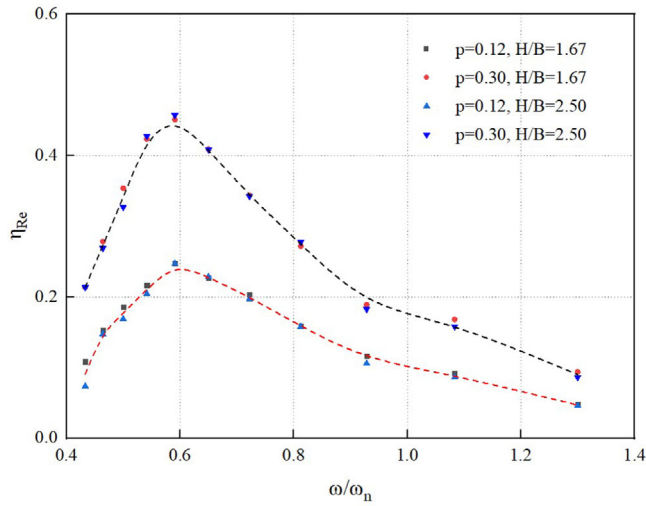


FIGURE 8 Variation of capture width ratio with ω/ω_n in regular waves

and linearity sequentially. The critical values of H/B for different modes are dependent on the hydraulic load value, similar to that for Z/H in Figure 7(a). Within the range of experimental test parameters, the larger the p value, the smaller the phase difference.

3.1.2 | Capture width ratio

Figure 8 shows the change curve of the captured width ratio, η_{Re} , with ω/ω_n . The subscript “Re” represents regular waves. Two wave heights ($H/B = 1.67$ and 2.50) were plotted and corresponded to the two hydraulic load values ($p = 0.12$ and 0.30). It can be seen from the test results that the η_{Re} value was related to both the frequency and load. For all of the working conditions shown in the figure, the variation trend of η_{Re} with the frequency rapidly increased to the maximum at first and then slowly decreased, and the optimal wave frequency was basically the same. The value of η_{Re} at $p = 0.3$ was larger than that at $p = 0.12$ on the whole, but whether there was a linear relationship still required further verification. Figure 9 further shows the variation of η_{Re} with p at three incident wave frequencies ($\omega/\omega_n = 0.50, 0.59, 0.81$). The wave height was constant at $H/B = 1.67$. The curve began from zero, that is, when $p = 0$, and the PTO did not capture the wave energy, even though the relative motion displacement is at its maximum (as shown in Figure 6). With an increase in the p value, η_{Re} increased first and then decreased. Under different wave frequencies, the optimal value of p at the corresponding η_{Re} was different. Based on the above results, the maximum value of η_{Re} measured in the experiment was 0.46 at $\omega/\omega_n = 0.59$ and $p = 0.20$.

3.2 | Irregular waves

The aforementioned parameter study under regular wave conditions was helpful to understand the motion and energy laws

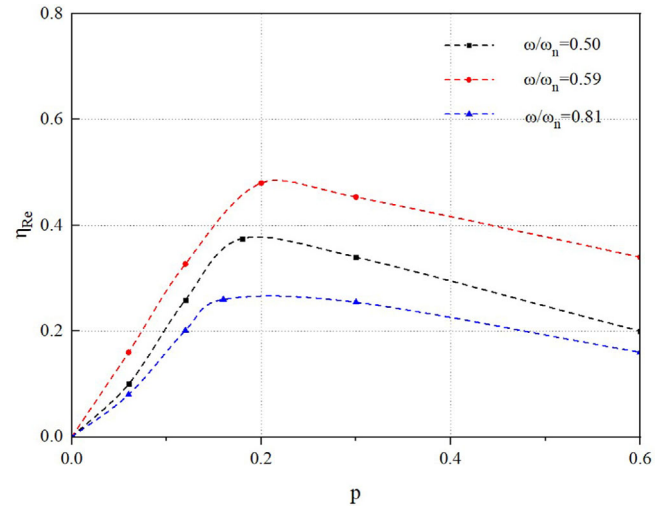


FIGURE 9 Variation of capture width ratio with p in regular waves at $H/B = 1.67$

of the device. However, under real sea conditions, waves are always in a random state. Therefore, in this section, the motion response and energy characteristics of the device under irregular incident waves were experimentally studied and compared with the test results of regular waves.

3.2.1 | The relative heave motion response

The spectrum, $S(\omega)$, is an empirical equation to quantitatively describe the energy distribution of random waves. In this experimental study, irregular waves in the flume were generated using the JONSWAP spectrum, which can be expressed using the following formula [51]:

$$S(\omega) = \frac{\beta_J H_S^2 \omega_p^4}{\omega^5} \exp\left[-\frac{5}{4} \left(\frac{\omega_p}{\omega}\right)^4\right] \cdot \gamma \times \exp\left[-(\omega/\omega_p - 1)^2 / 2\sigma^2\right] \quad (8)$$

where H_S is the significant wave height, and the corresponding characteristic wave period is denoted as T_S . They are the most important parameters used to characterize irregular waves. γ was a constant of 3.3 in this study, and the peak spectral frequency, ω_p , non-dimensional peak shape parameter σ , and the coefficient β_J had the following expressions:

$$\omega_p = \frac{2\pi \left[1 - 0.132(\gamma + 0.2)^{-0.559}\right]}{T_S} \quad (9)$$

$$\sigma = \begin{cases} \sigma_1 = 0.07 & \omega \leq \omega_0 \\ \sigma_2 = 0.09 & \omega > \omega_0 \end{cases} \quad (10)$$

$$\beta_J = \frac{0.006238}{0.230 + 0.0336\gamma - 0.185(1.9 + \gamma)^{-1} \cdot (1.094 - 0.019151 \cdot \ln \gamma)} \quad (11)$$

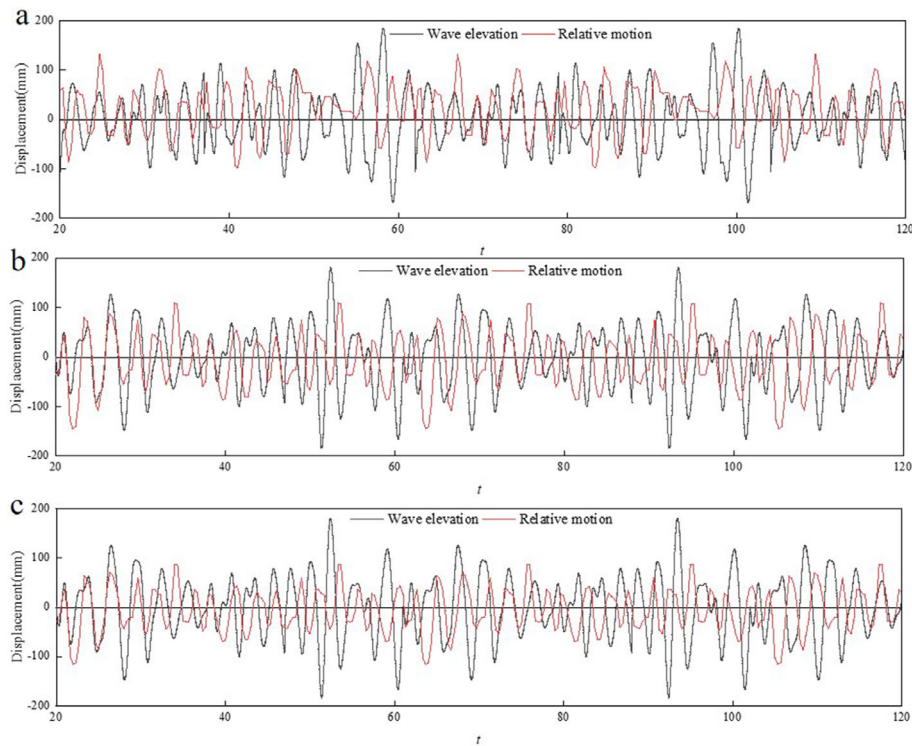


FIGURE 10 Time histories of wave elevation and relative motion in irregular waves, (a) $H_s = 0.3$ m, $T_s = 1.8$ s and $p = 0.12$; (b) $H_s = 0.3$ m, $T_s = 3.0$ s and $p = 0.12$; (c) $H_s = 0.3$ m, $T_s = 3.0$ s and $p = 0.20$

In the tests, a time series of 9000 records (300 s) was used in the Fourier analysis for each case. Figure 10 represents the time histories of the wave elevation and relative motion in the irregular waves under different wave conditions and external loads. The significant wave heights in the figure are $H_s = 0.3$ m, the wave energy periods are $T_s = 1.8$ s and $T_s = 3.0$ s, and the external loads are $p = 0.12$ and $p = 0.20$. It can be seen from the figure that, unlike the regular wave result, the relative motion no longer followed the wave elevation with a fixed period. In general, for the high wave heights, the relative motion period was close to the incident wave period, as shown in Figure 10(a) where $t = 55\text{--}67$ s and $t = 97\text{--}110$ s. For the other wave heights, relative motions had larger periods from the incident waves. Under the same wave parameters, the larger the load was, the worse the following performance of the relative motion with wave height was.

Different from the results that under regular waves, the relative heave motion has no fixed phase decay with the wave elevation (as can be seen from Figure 10), and only part of the incident waves can excite the model to generate heave motion. An analysis of more test results and the calculation of the ratio of relative motion generated, N_m , to the number of incident waves, N_w , during the test period of each group of parameters was conducted. The calculated results are shown in Figure 11. For each group of parameters described in the figure, the value of N_m/N_w increased with T_s , and the growth rate slowed down with an increase in the period. For $T_s = 1.2$ s and $H_s = 0.2$ m, there is only 57% of the incident waves under which the model can move in heave. While for $T_s = 3.0$ s and $H_s = 0.2$ m, there

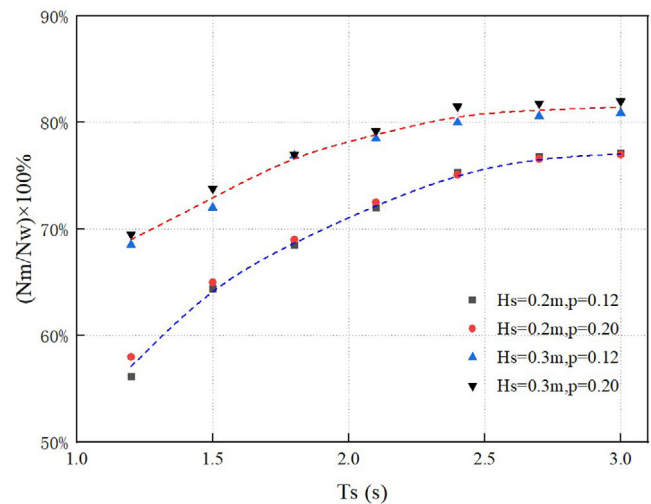


FIGURE 11 The effective fraction number of relative motion N_m/N_w varying with the characteristic wave period T_s for $H_s = 0.2, 0.3$ in irregular waves

is almost 77% of the incident waves that can excite the model motion. The N_m/N_w value at $H_s = 0.3$ m was larger than at $H_s = 0.2$ m, and the difference between the two decreased with an increase in the wave period. Under the same condition of H_s and T_s , the value of N_m/N_w at $p = 0.12$ and $p = 0.20$ are almost the same. Based on the above analysis, a high wave height and a long period are beneficial to the relative motion response of the model within the range of the test parameters.

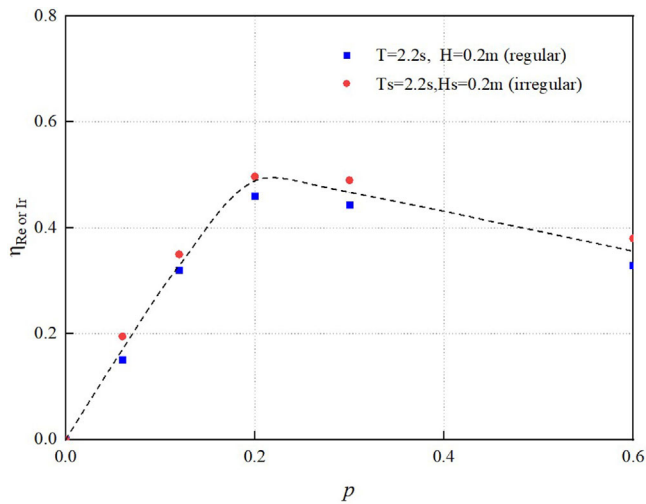


FIGURE 12 Variation of the capture width ratio η_{Ir} with p in irregular waves, $H_s = 0.2$ m, $T_s = 2.2$ s, regular wave results for comparison

3.2.2 | The capture width ratio in the irregular waves

For a random wave train with a spectrum of $S(\omega)$, the average wave energy density was approximated using the linear wave theory by the equation [52]:

$$E_b = \frac{1}{16} \rho g H_m^2 \quad (12)$$

where H_m is the characteristic wave height; and E_b denotes the averaged wave energy density calculated using the characteristic wave height. It has been proven that the linear wave method can accurately estimate the incident wave energy of a random sea state with appropriate characteristic wave height values [53]. Figure 12 shows the variation of η_{Ir} with a load, p , under irregular wave conditions of $H_s = 0.2$ m and $T_s = 2.2$ s. The test results of the regular waves with the same wave parameters are also plotted in the figure for comparison. As can be seen from the figure, the curve variation trend was very similar to that of the regular waves (Figure 9). However, the captured width ratio of the irregular waves was greater than that of the regular waves in the same situation. In Figure 13, the relationship between η_{Ir}/η_{Re} and the incident wave height (or significant wave height) was calculated. It can be seen that all of the results are greater than one, which indicates that under the same wave parameters, the capture width ratio of the irregular wave energy was greater than that of the regular wave energy. This result is significant for evaluating the error of the wave energy absorption when irregular wave states are represented by regular wave states.

4 | CONCLUSIONS

In this study, the motion response and energy characteristics of a hydraulic loaded two-body WEC under regular and irregular waves were studied using a series of flume experiments. By using

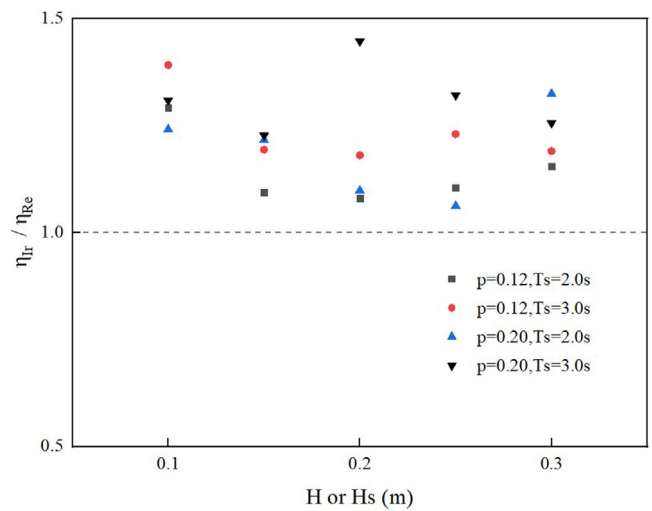


FIGURE 13 Comparisons of the capture width ratios of the experimental model in regular and irregular waves

a quantitative analysis of the influence of the wave height, frequency, and PTO load on the model response, the conclusions that follow were drawn:

1. Under the excitation of regular waves, the variation in the relative heave motion response of the hydraulic loaded two-body WEC with an incident wave height could be summarized into three modes. That is, linear, nonlinear, and non-moving modes. The initial moving line of the device was obtained. The critical values between the three motion modes were affected by the wave height and the PTO load value.
2. Under the excitation of irregular waves, the relative heave motion of the two-body WEC with hydraulic load primarily demonstrated two states of motion: a following motion with a similar value to the incident wave period and a delayed motion with a larger value than the wave period. This primarily depended on the instantaneous incident wave height and was affected by the load value.
3. In a regular wave environment, the capture width ratio of the system under different working conditions was analysed using the control variable method, and it was found that the maximum value of η_{Re} measured in the experiment was 0.46 at $\omega/\omega_n = 0.59$ and $p = 0.20$.
4. The captured power characteristics of the experimental model under irregular waves and regular waves had the same variation rule. For the same wave environments, the value, η_{Ir} , was always larger than that of η_{Re} , and the ratio range was approximately 110–145%. This result is instructive to analysing the error of wave energy absorption when irregular wave states are represented by regular wave states.

ACKNOWLEDGMENTS

This work was supported by the National Nature Science Foundation of China (U1706230) and the National Key R&D Program of China (2016YFE0205700).

ORCID

Shuang Wu  <https://orcid.org/0000-0002-7154-107X>

REFERENCES

- Falnes, J.: A review of wave-energy extraction. *Mar. Struc.* 20(20), 185–201 (2007)
- Zhang, Y.X., Zhao, Y. J., SUN, W., et al.: Ocean wave energy converters: Technical principle, device realization, and performance evaluation. *Renewable Sustainable Energy Rev.* 141, 110764 (2021)
- Jusoh, M.A., et al.: Hydraulic power take-off concepts for wave energy conversion system: A review. *Energies* 12(23), 4510 (2019)
- Babarit, A.: A database of capture width ratio of wave energy converters. *Renew. Energy*. 80(80), 610–628 (2015)
- Lopes, M.F.P., et al.: Experimental and numerical investigation of non-predictive phase-control strategies for a point-absorbing wave energy converter. *Ocean. Eng.* 36(36), 386–402 (2009)
- Margheritini, L., Vicinanza, D., Frigaard, P.: SSG wave energy converter: Design, reliability and hydraulic performance of an innovative overtopping device. *Renew. Energy*. 34(34), 1371–1380 (2009)
- Rusu, E., Guedes Soares, C.: Coastal impact induced by a pelamis wave farm operating in the Portuguese near shore. *Renew. Energy* 58(58), 34–49 (2013)
- Su, Y., You, Y., Zheng, Y.: Investigations on the oscillating buoy wave power devices. *China Ocean. Eng.* 16(1), 141–149 (2002)
- Nielsen, K., Smed, P.E.: Point absorber optimization and survival testing. In: *Proceedings of the Third European Wave Energy Conference*, Patras, Greece (1998)
- Weinstein, A., et al.: Aqua Buoy-the offshore wave energy converter numerical modeling and optimization. In: *Proceedings of MTTs/IEEE Techno-ocean'04 Conference*, Kobe, Japan (2004)
- Eriksson, M., et al.: Wave power absorption: Experiments in open sea and simulation. *J. Appl. Phys.* 102(102), 084910 (2007)
- Zuo, L., et al.: On the dynamics and design of a two-body wave energy converter. *Renewable Energy* (101), 265–274 (2017)
- Falcao, A.F.O.: Wave energy utilization: A review of the technologies. *Renew. Sustain. Energy. Rev.* 14(3), 899–918 (2010)
- Lopez, I., et al.: Review of wave energy technologies and the necessary power-equipment. *Renew. Sustain. Energy*. 27, 413–434 (2013)
- Sheng, W., Alcorn, R., Lewis, T.: Physical modeling of wave energy converters. *Ocean. Eng.* 84(84), 29–36 (2014)
- Berggren, L., Johansson, M.: Hydrodynamic coefficients of a wave energy device consisting of a buoy and a submerged plate. *Appl. Ocean Res.* 14(1), 51–58 (1992)
- Eidsmoen, H.: Hydrodynamic parameters for a two-body axisymmetric system. *Appl. Ocean Res.* 17(2), 103–115 (1995)
- Zheng, Y.H., et al.: Hydrodynamic properties of two vertical truncated cylinders in waves. *Ocean Eng.* 32(3), 241–271 (2005)
- Weinstein, A., et al.: AquaBuOY-the offshore wave energy converter numerical modeling and optimization//OCEANS'04. MTTs/IEEE TECHNO-OCEAN'04. *IEEE* 4, 1854–1859 (2004)
- Engström, J., et al.: Wave energy converter with enhanced amplitude response at frequencies coinciding with Swedish west coast sea states by use of a supplementary submerged body. *J. Appl. Phys.* 106(6), 064512 (2009)
- Vicente, P.C., Falcão, A.O., Justino, P.A., Non-linear slack-mooring modelling of a floating two-body wave energy converter. *The European Wave and Tidal Energy Conference*, Southampton, England, January (2011), pp. 1–10
- Cândido, J.J., Justino, P.A.P.S.: Modelling, control and pontryagin maximum principle for a two-body wave energy device. *Renewable Energy* 36(5), 1545–1557 (2011)
- Bijun W., Xing W., Xianghong D.: Response and conversion efficiency of a wave energy device consisting of double cylindrical floats with two degrees of freedom. *Sci. Sin. Phys., Mech. Astron.* 43(8), 978–986 (2013)
- Liqun L., Chunxu W., Bijun W.: Study on power conversion features of the two-buoy wave energy device. *J. Shanghai Univ.* 23(3), 475–480 (2014)
- Ruehl, K.: Time-domain modeling of heaving point absorber wave energy converters, including power take-off and mooring. Master Thesis, Oregon State University, (2011)
- Wacher, A., Nielsen, K., Mathematical and numerical modeling of the AquaBuOY wave energy converter. *Mathematics in Industry Case Studies.* 2, pp. 16–33 (2010)
- Chau, F.P., Yeung, R.W.: Inertia, damping, and wave excitation of heaving coaxial cylinders. In: *Proceedings OMAE 2012–83987*, Brazil, pp. 803–813 (2012)
- Cho I.H., Kim M.H.: Hydrodynamic performance evaluation of a wave energy converter with two concentric vertical cylinders by analytic solutions and model tests. *Ocean Eng.* 130(15), 498–509 (2017)
- Zheng, S., Zhang, Y., Sheng, W.: Maximum wave energy conversion by two interconnected floaters. *J Energy Resour Technol* 138(3), 032004 (2016)
- Zheng, S., Zhang, Y., Iglesias, G.: Concept and performance of a novel wave energy converter: Variable Aperture Point-Absorber (VAPA). *Renewable Energy* 153(C), 681–700 (2020)
- Jin P., Zhou B., etal M.G., : Performance optimization of a coaxial-cylinder wave energy converter. *Energy* 174, 450–459 (2019)
- Vantorre, M., Banasiak, R., Verhoeven, R.: Modelling of hydraulic performance and wave energy extraction by a point absorber in heave. *Appl. Ocean Res.* 26(1), 61–72 (2007)
- Bjarte-Larsson, T., Falnes, J.: Laboratory experiment on heaving body with hydraulic power take-off and latching control. *Ocean Eng.* 33(7), 847–877 (2006)
- Waters, R., et al. Experimental results from sea trials of an offshore wave energy system. *Appl. Phys. Lett.* 90(3), 034105 (2007)
- Payne, G.S., et al.: Assessment of boundary-element method for modelling a free-floating sloped wave energy device. Part 2: Experimental validation. *Ocean Eng.* 35(3), 342–357 (2008)
- Kramer, M., Marquis, L., Frigaard, P.: Performance evaluation of the wavestar prototype. In: *The 9th European Wave and Tidal Energy Conference: EWTEC 2011*, Southampton, UK (2011)
- Falcao, A.F.O., Pereira, P.E.R., Henrique, J.C.C.: Hydrodynamic simulation of a floating wave energy converter by a U-tube rig for power take-off testing. *Ocean. Eng.* 37(37), 1253–1260 (2010)
- Cen Y.: Study on operating characteristics of oscillating-buoy wave energy converter. PhD thesis, Tsinghua University (2015)
- Beatty, S.J., et al.: Experimental and numerical comparisons of self-reacting point absorber wave energy converters in regular waves. *Ocean Eng.* 104(104), 370–386 (2015)
- Beatty, S.J., et al.: Experimental and numerical comparisons of self-reacting point absorber wave energy converters in irregular waves. *Ocean Eng.* 173, 716–731 (2019)
- Kim S.-J., Koo W., Shin M.-J.: Numerical and experimental study on a hemispheric point-absorber type wave energy converter with a hydraulic power take-off system. *Renewable Energy* 135(135), 1260–1269 (2019)
- Son D., Belissen V., Yeung R.W.: Performance validation and optimization of a dual coaxial-cylinder ocean-wave energy extractor. *Renewable Energy* 92, 192–201 (2016)
- Jin, C., et al.: Performance estimation of resonance-enhanced dual-buoy wave energy converter using coupled time-domain simulation. *Renewable Energy* 160, 1445–1457 (2020)
- Cargo, C.: Design and control of hydraulic power take-offs for wave energy converters. PhD thesis, University of Bath (2012)
- Ocean Power Technologies, <http://www.oceanpowertechnologies.com/>, accessed 27 November 2015
- Cen Y., Yongliang Z.: Experimental study on operation performance of wave-driven pressure pump. *J. Hydraul. Eng.* 44(9), 1107–1111 (2013)
- Falcao A.F.O.: Modelling and control of oscillating-body wave energy converters with hydraulic power take-off and gas accumulator. *Ocean Eng.* 34(10), 2021–2032 (2007)
- Falnes J.: *Ocean Waves and Oscillating Systems: Linear Interactions Including Wave-energy Extraction*. Cambridge University Press, Cambridge UK (2002)
- Faltinsen, O.: *Sea Loads on Ships and Offshore Structures*. Cambridge University Press, Cambridge UK (1990)
- Chakrabarti, S.K.: *Developments in Offshore Engineering, Wave Phenomena and Offshore Topics*. Gulf Professional Publishing, Houston, USA, pp. 295–335 (1999)

51. Payne, G.S., Taylor, J.R., Ingram, D.: Best practice guidelines for tank testing of wave energy converters. *J. Ocean Technol.* 12(4), 39–69 (2009)
52. Goda Y.: *Random Seas and Design of Marine Structures*, World Scientific Publishing Co. Pte. Ltd, Singapore (2000)
53. Zang, Z., et al.: Hydrodynamic responses and efficiency analyses of a heaving-buoy wave energy converter with PTO damping in regular and irregular waves. *Renewable Energy* 116(Part A), 527–542 (2018)

How to cite this article: Wu, S., Liu, Y., Qin, J.: Experimental analyses of two-body wave energy converters with hydraulic power take-off damping in regular and irregular waves. *IET Renew. Power Gener.* 15, 3165–3175 (2021).

<https://doi.org/10.1049/rpg2.12218>